

Seismic design and assessment of steel-concrete frame structures with welded dissipative fuses

Luís Calado, Jorge M. Proença* and João Sio

Department of Civil Engineering, Instituto Superior Técnico, U Lisboa, and CERIS, Av. Rovisco Pais, 1049-001 Lisboa, Portugal

(Received October 23, 2019, Revised March 13, 2020, Accepted April 3, 2020)

Abstract. This research presents the design and numerical assessment of composite steel-concrete frame structures with welded dissipative fuses. The assessment has been carried out based on linear response spectrum, nonlinear static pushover and time history procedures. The analytical expressions which define the envelope of the nonlinear response of the dissipative fuses are first presented and calibrated against experimental results available in literature. The assessment is then carried out according to a design methodology proposed herein. Outcomes of the numerical assessment indicate that the use of welded dissipative fuses successfully limited damage within the replaceable parts. Furthermore, although structures with dissipative fuses present lower strength and, generally, lower displacement capacity, their displacement ductility and global dissipative performance are generally higher than conventional structures, especially when the structure with dissipative fuses presents a dissipative configuration adjusted to the bending moment distribution diagram calculated for the applied seismic action.

Keywords: welded dissipative fuses; repairability; numerical model; seismic design; earthquake resistant frames

1. Introduction

Current code provisions allow structures to be designed to withstand earthquakes by developing extensive plastic deformations in specifically assigned dissipative areas provided that structural integrity is not compromised. Compared to an elastic design, this approach considerably reduces the design seismic forces, resulting in a more efficient use of building resources. However, two major concerns arise when the aforementioned design philosophy is employed.

The first concern relates to the global ductility supply of the structure, which must be sufficient to cope with the demand imposed by an earthquake. In this regard, the Northridge (USA 1994) (Engelhardt and Sabol 1997) and Hyogoken-Nanbu (Kobe, Japan 1995) (Nakashima *et al.* 1998) earthquakes are examples which highlight the severity of not achieving the required ductility within the connections of a structure. The high concentration of stresses and the premature fracture of the welds within the connections substantially reduced the global ductility supply of some structures, leading to their collapse during the earthquakes.

Following those events, strengthening and weakening strategies have been proposed to improve the seismic performance of beam-to-column connections (Mazzolani 2000). The strengthening strategy is achieved by adding reinforcements to the connection itself (Engelhardt and Sabol 1998), such as cover plates and haunches, or by expanding the beam flanges at the beam ends (Ma *et al.*

2019). The weakening strategy consists of reducing the cross section of the beam a short distance from its connection with the column [termed as the Reduced Beam Section strategy, RBS (Plumier 1990, 2000, Yu and Uang 2001, Pachoumis *et al.* 2010)]. However, as with conventional connections, both solutions still consider the structural beam to be the main source of energy dissipation through the extensive development of plastic deformations. Therefore, in the aftermath of an earthquake, the reparation of structures adopting these solutions is often costly and time-consuming (i.e. the second concern of the plastic design philosophy).

As international interest increased in designing structures not only for collapse prevention but also from an economic and sustainable standpoint, researchers began to draft new replaceable solutions for beam-to-column connections. Ozkaynak *et al.* (2018) proposed a dissipative steel cushion which was initially applied for concrete structures but can be extended for more general purposes. For steel structures, Balut and Gioncu (2003) and Jiang *et al.* (2019) conceived replaceable fuses similar to the “dog-bone” solution of the RBS strategy, which were mainly applied for I-beam-to-column connections. Sabbagh *et al.* (2013) developed an equivalent fuse for I-beam-to-CHS-column connections. Lopez-Barraza *et al.* (2016) proposed a self-centring moment resistant frame solution using post tensioned connections. These connections were conceived to dissipate energy and to facilitate post-earthquake repairs. Fewer solutions were developed for steel-concrete structures (Koetaka *et al.* 2005, Oh *et al.* 2009, He *et al.* 2018). Steel-concrete structures can provide further energy dissipation capacity compared to steel structures due to the possibility of energy dissipation in the shear connections between the steel beam and the concrete slab (Vasdravellis *et al.* 2009). Although the above-mentioned solutions for

*Corresponding author, Ph.D., Associate Professor
E-mail: jorge.m.proenca@tecnico.ulisboa.pt

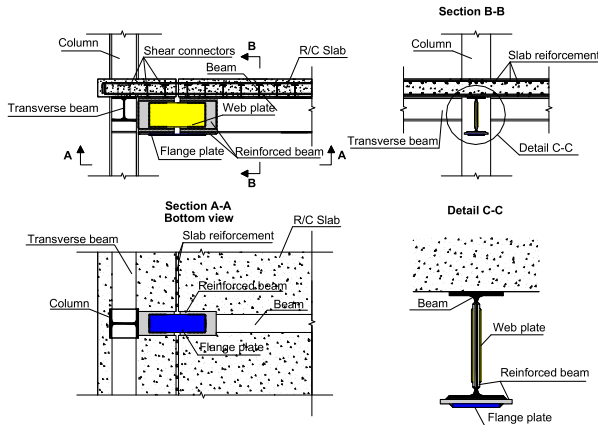


Fig. 1 Partial illustration of moment-resisting frame structures equipped with welded dissipative fuses (Calado *et al.* 2013)

steel-concrete structures present reduced strength degradation due to the damage of the concrete slab, permanent damage is still inevitable.

In this respect, the welded and bolted dissipative fuses developed during the FUSEIS project (Castiglioni *et al.* 2012, Calado *et al.* 2013) present the advantage of preventing major cracking of the concrete slab through the addition of a gap at the fuse location. The welded solution, which is illustrated in Fig.1, entails the interruption of the composite steel-concrete beam at both ends. Depending on the chosen solution, the connection is then re-established with welded or bolted flange and web fuse plates. The effective transmission of bending moment is achieved with the set of binary forces mobilised by the flange plate and the reinforcing steel bars (rebars) of the concrete slab.

The rebars were left intact when the discontinuities of the beam were introduced. Given that the rebars cannot be replaced, these should be designed to remain elastic at all times. The length of the discontinuities of the beam is defined such that they allow the development of large rotations within the fuse plates without causing major damage to the concrete slab through concrete-to-concrete contact. Finally, the area adjacent to the fuses is reinforced with additional steel plates to prevent any spread of damage to the non-replaceable parts of the composite beam.

Subsequent to the experimental testing of the welded and bolted dissipative fuses at the Instituto Superior Técnico (IST) of the University of Lisbon and at the Politecnico di Milano, numerical investigations and drafting of design strategies were carried out. Two types of numerical investigations with the welded and bolted dissipative fuses were performed by Valente *et al.* (2016, 2017a, b): i) a detailed three-dimensional finite element (FE) analyses for calibration purposes; and ii) nonlinear time history analyses of multi-storey buildings equipped with the experimental fuses.

This research provides a design-oriented investigation of composite steel-concrete frame structures equipped with welded dissipative fuses. The analytical expressions which define the moment-rotation envelop of the dissipative fuse are first reviewed and discussed.

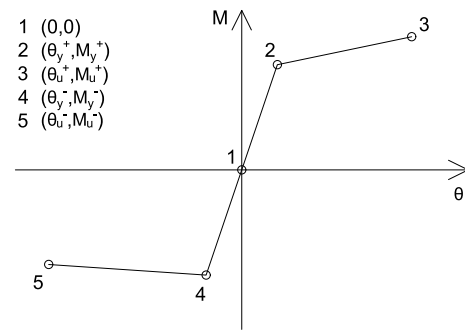


Fig. 2 Schematic illustration of the moment-rotation curve of welded dissipative fuses

A design strategy suitable for adaptation under current code provisions is then proposed, being subsequently assessed based on numerical analyses of case study structures. These numerical analyses also serve to assess the seismic performance of structures equipped with welded dissipative fuses to conventional moment-resisting frame structures.

2. Analytical characterisation of the moment-rotation curve of welded dissipative fuses

Fig. 2 illustrates the typical moment-rotation curve proposed for the fuse according to recent researches. The curve is composed of three linear segments with a total of 5 characteristic points: (1) is the origin; (2) and (3) are the yield and ultimate sagging rotations; (4) and (5) are the yield and ultimate hogging rotations. These are determined with a set of analytical expressions considering the behaviour of the fuse observed during the experimental programme (Calado *et al.* 2013).

2.1 Sagging yield bending moment and rotation

The yield bending moment of the fuse can be calculated based on the cross section illustrated in Fig. 3, involving the geometric and mechanical properties of the rebars and of the flange fuse plate. The following major assumptions have been made: i) linear strain distribution and ii) disregard of the contribution of the web plates to the bending moment.

According to Fig. 3, x_{cg} is the distance from the upper rebar layer to the centre of gravity of the cross section, d is the distance between the upper and lower rebar layers, and h is the length from the upper rebar layer to the flange plate.

When x_{cg} is known, the strain of the upper and lower rebar layers, $\epsilon_{rebar,upp}$ and $\epsilon_{rebar,low}$, respectively, can be calculated by following the linear strain diagram and imposing the yield strain for the flange plate ($\epsilon_{flange} = f_y/E$, where f_y is the yield stress and E is the elastic modulus).

The axial force of each component can then be

Table 1 Properties for the welded dissipative fuses studied within the experimental campaign

		Assumed value	Comment
Upper and lower rebar layers	A_i	$A_{rebar,upp \text{ or } low}$	-
	$A_{v,i}$	$0.6 \cdot A_{rebar,upp \text{ or } low}$	An area reduction of 40% is considered for the circular section to match the provisions of EN1993-1-8 (3.6.1) (Eurocode 2005) for the shear area of bolts.
	$L_{d,i}$	Rebar gap + 100 mm	The additional 100 mm accounts for the possible loss of adhesion between the rebars and the concrete.
Web and flange fuse plates	A_i	$A_{web \text{ or } flange}$	-
	$A_{v,i}$	$A_{web \text{ or } flange}$	-
	$L_{d,i}$	$L_{f,flange} + \text{weld length}$	The flexibility of the welds is implicitly considered by assuming the deformable length as the total length of the fuse plates.

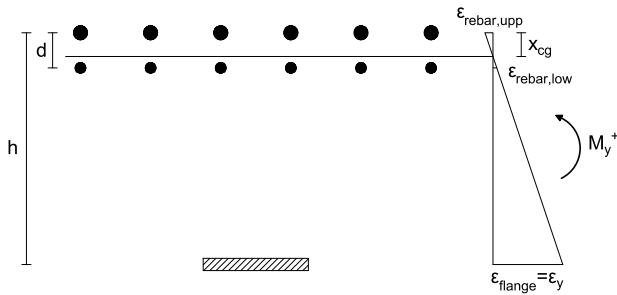


Fig. 3 Schematic illustration of yield moment model

determined, leading to the calculation of the yield moment, which can be given by Eq. (1)

$$M_y^+ = F_{flange} \cdot h + F_{rebar,low} \cdot d \quad (1)$$

The yield rotation θ_y^+ is obtained by dividing the corresponding yield moment by the initial rotational stiffness $K_{WFBS,ini}$ of the dissipative fuse

$$\theta_y^+ = \frac{M_y^+}{K_{WFBS,ini}} \quad (2)$$

Calado *et al.* (2013) proposed an initial stiffness model based on the component method specified in EN1993-1-8 (Eurocode 2005). The model, shown in Fig. 4, comprises four basic components $K_{rebar,upp}$, $K_{rebar,low}$, K_{web} and K_{flange} , representing the stiffness contribution of the upper and lower rebar layers, web and flange fuse plates, respectively.

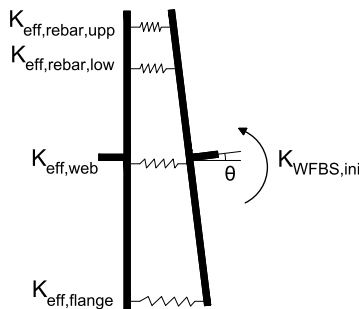


Fig. 4 Schematic illustration of stiffness model

Each basic component is composed of two linear springs in series, which characterise their axial and shear deformability

$$K_{eff,i} = \frac{1}{\frac{1}{K_{axial,i}} + \frac{1}{K_{shear,i}}} \quad (3)$$

Eqs. (4) and (5) are used to estimate the value of the axial $K_{axial,i}$ and shear $K_{shear,i}$ stiffness.

$$K_{axial,i} = \frac{E \cdot A_i}{L_{d,i}} \quad (4)$$

$$K_{shear,i} = \frac{0.38 \cdot E \cdot A_{v,i}}{\beta \cdot z_i} \quad (5)$$

where E is the elastic modulus, A_i , $A_{v,i}$, $L_{d,i}$ are the cross section area, the shear area and the deformable length of the component i , respectively; z_i is the lever arm of the shear forces which is considered equal to the deformable length; β is the transformation parameter specified in EN1993-1-8 (Eurocode 2005) and, since the bending moments on both sides of the fuse have approximately the same direction and value, it is taken as 1.0. Table 1 shows the values chosen for the aforementioned quantities and the corresponding comment.

The equation adapted from EN1993-1-8 (6.3.1) (Eurocode 2005) to compute the initial rotational stiffness of the welded dissipative fuse can be shown to be given by Eq. (6)

$$K_{WFBS,ini} = \sum K_{eff,i} \cdot h_i^2 \quad (6)$$

where $h_i = d_i - z_{cs}$ is the vertical distance between the position of the component d_i and the centre of stiffness z_{cs} .

2.2 Sagging ultimate bending moment and rotation

Disregarding the web plates, the ultimate moment can be approximately calculated by assuming the development of the ultimate stress in the flange plate and a lever arm equal to the distance between the plate and the geometric centre of the upper rebar layer, h (Fig. 5, Eq. (7))

This conservative approach assumes that the plastic neutral axis lies near the position of the lower rebar layer, which results in a negligible moment resistance contribution

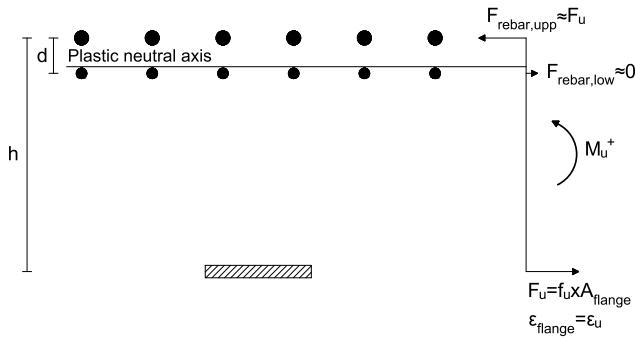


Fig. 5 Schematic illustration of ultimate moment model

from the lower rebar layer. In the case of a single rebar layer dissipative fuse, which is usually applied to a composite steel-concrete beam with corrugated slabs, Eq. (7) gives the exact outcome for the assumed analytical model.

$$M_u^+ = f_u \cdot A_{flange} \cdot h \quad (7)$$

The non-yield condition is considered to be implicitly satisfied for the lower rebar layer, whereas the upper rebar layer should comply with the following condition

$$\sigma_{rebar,upp} = \frac{f_u \cdot A_{flange}}{A_{rebar,upp}} \quad (8)$$

where the $\sigma_{rebar,upp}$ should be lower than the yield stress of the rebars, f_{sd} , for conveniently designed fuses.

The corresponding rotation θ_u^+ is assumed to be given by Eq. (9)

$$\theta_u^+ = \frac{\varepsilon_u + \varepsilon_{rebar,upp}}{h} \cdot L_{f,flange} \quad (9)$$

where h is represented in Fig. 5, $L_{f,flange}$ is the free length of the flange plate and ε_u is the ultimate strain considered for the steel of the flange plate. $\varepsilon_{rebar,upp}$ is the strain at the upper rebar layer, calculated by $\sigma_{rebar,upp}/E$ (where E is the Young's modulus of the rebars).

2.3 Hogging yield bending moment and rotation

The hogging yield moment can be calculated using the same model described for the sagging branch. However, since the flange plate buckles under compression, its compressive resistance may reduce, which in turn decreases the bending moment resistance of the dissipative fuse. The analytical model shall therefore account a plastic buckling mechanism such that the phenomenon is reproduced accordingly. Calado *et al.* (2013) adapted Gomes and Appleton (1997) buckling model for a compressed steel rebar to achieve this objective. The mechanism of the model is illustrated in Fig. 6 and can be shown to be expressed by Eq. (10) (Gomes and Appleton 1997).

$$\sigma_b = \frac{2\sqrt{2} \times M_{Rd,flange}}{A_{flange} \times L_0} \times \frac{1}{\sqrt{\varepsilon}} \quad (10)$$

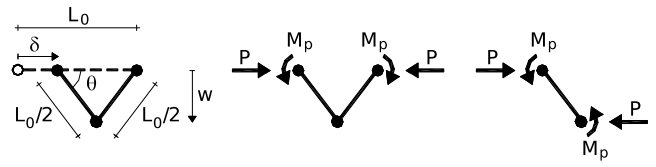


Fig. 6 Schematic illustration of plastic buckling model (adapted from Calado *et al.* 2013)

where σ_b , $M_{Rd,flange}$, L_0 and ε are the buckling stress, the bending moment resistance, the buckling length (taken as the free length $L_{f,flange}$) and the strain of the flange plate, respectively.

$M_{Rd,flange}$ should consider the interaction between the compression and bending of the flange plate. Similarly to the procedure adopted for a circular cross-section in Gomes and Appleton (1997), this interaction can be shown to be expressed by Eq. (11) for a rectangular cross-section

$$\sigma_{b,interaction} = \frac{-1 + \sqrt{1^2 + 4 \cdot z^2 \cdot y \cdot M_{pl,Rd,flange}}}{2 \cdot z \cdot y \cdot A_{flange}} \quad (11)$$

with

$$y = \frac{1}{4 \cdot b \cdot f_y} \quad (12)$$

$$z = \frac{2\sqrt{2}}{L_{f,flange} \cdot \sqrt{\varepsilon}} \quad (13)$$

where $M_{pl,Rd,flange}$ and b are the bending moment resistance and the width of the flange plate, and f_y is the yield stress of the steel material.

The tensile stress-strain curve of the steel is intersected by the asymptotic curve to determine the modified compressive stress for the flange plate. However, since a maximum value equal to f_y is imposed, the final stress and strain values are given by Eqs. (14) and (15), respectively

$$\sigma_{flange} = \min\{\sigma_{b,interaction}, f_y\} \quad (14)$$

$$\varepsilon_{flange} = \min\{\varepsilon, \varepsilon_y\} \quad (15)$$

The yielding rotation at hogging configuration is assumed as

$$\theta_y^- = \frac{M_y^-}{K_{WFBS,ini}} \quad (16)$$

2.4 Hogging ultimate bending moment and rotation

The hogging ultimate moment is considered to be given by the expression adapted from Eq. (7)

$$M_u^- = \sigma_{u,flange}^- \cdot A_{flange} \cdot h \quad (17)$$

with

$$\sigma_{u,flange}^- = (1 - \beta) \cdot f_u + \beta \cdot \sigma_{b,interaction}(\varepsilon_u) \quad (18)$$

Eq. (18) considers the plastic buckling of the flange plate and the strain hardening phenomena to be concurrent. Their influence on the ultimate compressive stress of the flange plate is represented by the coefficient β , whose values range from 0 to 1. β is herein taken as 0.65 through calibration based on the experimental results provided in Calado *et al.* (2013). The former equation serves as a correction of the original Gomes and Appleton (1997) based approach to consider the kinematic strain hardening effects at the ultimate strain.

Lastly, the ultimate hogging rotation value is considered identical to that estimated for the sagging branch.

2.5 Model calibration and validation

Table 2 gives the geometric and material properties of the welded dissipative fuses studied within the experimental campaign. These serve as reference values for the calibration and assessment of the proposed analytical models.

Calibration was carried out by adjusting the cyclic loading curve obtained from a time history analysis of a vertical cantilever with the fuse located at its fixed end to the one registered during the experimental programme.

The fuse is simulated by means of a link element, whose nonlinear behaviour is characterised by a moment-rotation envelope, defined by the analytical models previously proposed, and by a chosen type of hysteresis. Pivot hysteresis (Dowell *et al.* 1998) is employed because it can capture different pinching behaviours during load reversals through careful calibration of its parameters.

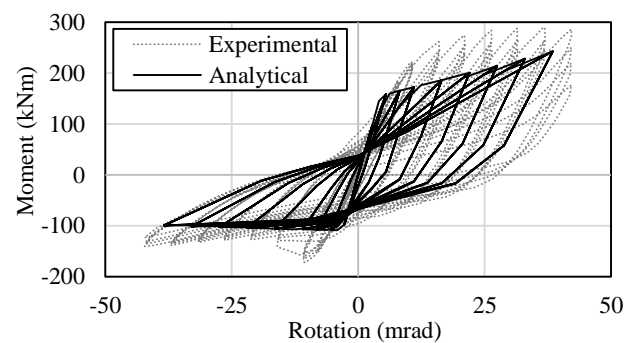
Figs. 7(a)-7(c) illustrates the calibration results for the welded dissipative fuses equipped with flange plates B, E and F, respectively. Overall, the analytical curves fit reasonably with those obtained experimentally, with underestimated resistance values observed within B and F cases. The underestimation of the resistance values may be mainly attributed to the fact that the bending moment contribution of the web plates was disregarded in the resistance models.

The web plates were capacity designed to resist the shear force corresponding to the highest bending moment for the set of flange plates that were tested. The resulting dimensions were then kept constant throughout the rest of the experimental tests. Thus, the percentage of the web plate area required to withstand the shear forces is expected to increase with the bending moment resistance of the dissipative fuse based on equilibrium and a more accurate analytical estimate should be achieved, since the remaining contribution of the web plates to the ultimate bending moment becomes negligible. Notwithstanding, since the assumed model underestimates the experimental resistance values, the model provides a conservative design approach for the welded dissipative fuse in terms of its resistance. However, caution is needed when capacity designing the non-dissipative elements if the web plates are to be oversized for their purpose, since the design internal forces and moments of the non-dissipative elements depend on the bending moment resistance of the dissipative fuse.

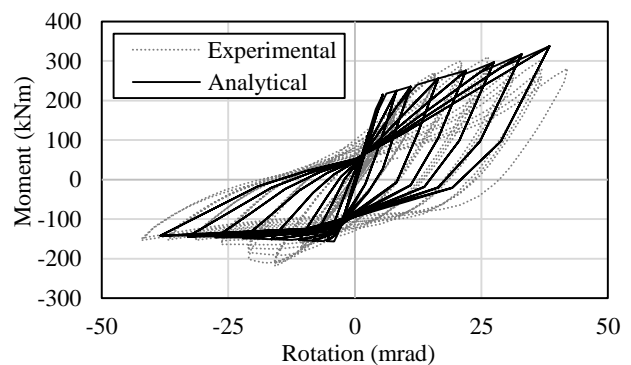
A model which considers the interaction between the bending moment and the shear force occurring within the web

Table 2 Input data for model calibration and assessment

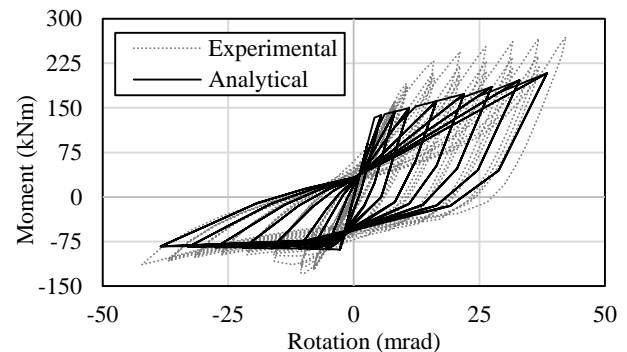
		Dimension (mm, mm ²)	Material
Gap	Rebar	50	-
	Beam	50	-
Web and flange fuse plate length	Total	470	-
	Free	170	-
Rebar layer within the effective width	Upper	15 Φ 20	A500
	Lower	8 Φ 16+6 Φ 12	
Fuse plates	Web	2x 230*4	S275
	Flange B	130*10	
	Flange E	150*12	
	Flange F	140*8	



(a) Specimen with flange plate B



(b) Specimen with flange plate E



(c) Specimen with flange plate F

Fig. 7 Model calibration and validation

plates would improve the results. However, it implies increased computational demand and difficulty in design

because the determination of the bending moment resistance would be implicit, therefore requiring the use of iterative procedures.

In this respect, two practical approaches to satisfy the requirements imposed by the capacity design of non-dissipative elements could be: i) to define the web plates as a function of the dimension of the flange plate and ii) to apply a more conservative overstrength ratio to the design forces of the non-dissipative elements.

Regarding the initial stiffness of the dissipative fuse, the proposed component method generally yielded good approximation, but slightly overestimated the stiffness of the fuse equipped with flange plate E. The difference may be attributed to the fact that the experimental values have been reduced by the deterioration of the non-replaceable parts with the number of testing (Calado *et al.* 2013).

In terms of the component ductility supply, the ultimate rotations predicted by the analytical model had values slightly lower than those registered in the experimental tests, but higher than the minimum rotation required for ductility class high (DCH) according to EN1998-1 (Eurocode 2004b).

3. Proposed design methodology

Since the main aim of the design is to circumscribe the development of plastic deformations within pre-defined dissipative zones, the proposed design methodology is similar to that described for conventional moment-resisting frame structures in EN1998-1 (Eurocode 2004b). Therefore, one of the tasks, concerning the welded dissipative fuse, was to propose a set of appropriately rearranged clauses with the purpose of including its usage within EN1998-1 (Eurocode 2004b). The outcome of such work is reported in Calado *et al.* (2017) and is used in the present research as the basis for verifying structures equipped with welded dissipative fuses.

Designing structures to withstand seismic actions is more difficult because of the uncertainty of their effects in terms of interior forces. The severity of the action depends on the mechanical characteristics of the structural elements, which in turn are defined based on the acting forces and moments. The design of moment-resisting frame structures with welded dissipative fuses is therefore an iterative process, but the number of iterations required can be reduced if a reasonable starting point is chosen. The design may start by defining the gravity load members, assuming a structure without the dissipative fuses (i.e. conventional structure). A seismic assessment using the response spectrum method (Eurocode 2004b) can then be performed to get an initial idea of the global stiffness and internal forces in the structure. The behaviour factor employed within the response spectrum method should be based on the expected ductility supply of the structure equipped with the dissipative fuses, which, as reported in Calado *et al.* (2017), can be initially assumed as four. The resulting conventional structure should have sufficient stiffness and overstrength against the design seismic action such that the change in demand caused by the introduction of the dissipative fuses at later stages will make it unnecessary to perform a complete re-design of the structure.

With the conventional structure defined, the value of bending moments obtained from its response spectrum analysis is used to design the dissipative fuses. The fuses have been conceived to resist mainly the lateral loads of the structure, and therefore should be placed near the null moment sections defined by the gravity loads applied to the structural beams. The hysteretic behaviour of the fuses can then be computed with the analytical model described in the previous section, to gather all the necessary information for the verification and assessment of the structure equipped with the dissipative fuses through the usual design code procedures (i.e., linear response spectrum, nonlinear static and dynamic analyses) (Eurocode 2004b, Calado *et al.* 2017). In particular, the behaviour factor employed in the response spectrum analyses can be validated based on the outcomes of the nonlinear static and dynamic analyses, which provide data regarding the ductility of the structure. A re-design will be needed if the structure does not satisfy the imposed seismic requirements or the behaviour factor initially chosen is well in excess of the verification value.

4. Numerical assessment of case study structures

2-, 4- and 8-storey composite steel-concrete moment-resisting frame structures (Fig. 8) were numerically assessed to compare the seismic behaviour of conventional frame structures and of those equipped with the dissipative fuse. For each building height, three different dissipative configurations that highlight the method of dissipation used by the frame structure were considered: i) conventionally designed structures (i.e., structures without dissipative fuses); ii) structure equipped with the same fuse section for all storeys, which is controlled by the maximum bending moment obtained at all storeys (generally governed by the lower storeys); and iii) structure with several fuse sections introduced according to a general bending moment distribution diagram. The bending moment distribution diagram was obtained from a response spectrum analysis of a structure without dissipative fuses. The naming example used hereinafter to identify the case studies is 2-C, with 2 being the number of storeys (2, 4, 8) and C being the type of dissipative configuration (C – conventional, W1 – one defined fuse section, W2 – several fuse sections). The conventional structures, which were then served as basis for the design of W1 and W2 structures, were designed according to EN1998-1 (Eurocode 2004b) for a target peak ground acceleration of 0.5g. All structures were composed of four identical frames [Fig. 8(a)] in which their I-shaped columns function on their strong moment of inertia axes.

The structure had a constant storey height of 3.5 meters and was composed of four seven-meter span bays, spaced seven meters in the transverse direction, thus giving a 21 by 28-metre floor plan with square slab panels [Fig. 8(b)]. The main beams forming these 4-bay frames were identical to those which connect them in the perpendicular direction.

Two additional rows of secondary beams were considered between adjacent 4-bay frames, parallel to their direction and supported by the main beams in the perpendicular direction. The sole purpose of the secondary beams is to help support the

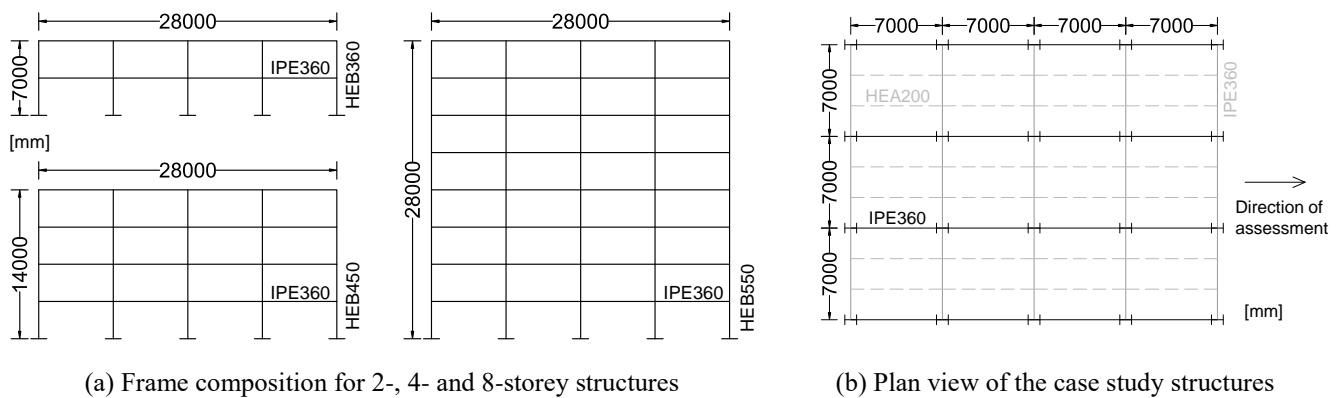


Fig. 8 Geometric considerations for the case study structures

composite steel-concrete corrugated slab (Fig. 9) and did not contribute to the lateral force resistant system of the structure.

Despite presenting three-dimensional structures, a planar numerical assessment was subsequently performed to study the lateral resistance capacity and ductility of the case studies only in the direction of the 4-bay frames [see Fig. 8(b)]. Composite action of the slab was assumed for both the main and secondary beams, which had IPE360 and HEA200 assigned steel profiles, respectively. Each structural height comprised an identical column profile on every storey, which was HEB360, HEB450 and HEB550 for the 2-, 4- and 8-storey buildings, respectively. Material properties are given in Fig. 9 for the composite steel-concrete slab and a steel grade of S355 was assumed for all beams and columns.

With respect to dissipative fuses, these were conceived for four main levels of bending moment resistance. Each level was further divided into dissipative fuses located in interior and exterior frames due to effective width considerations for the concrete slab. The effective widths of the concrete slab were determined according to EN1994-1-1 (Eurocode 2004a) assuming the zone of negative bending moments. This resulted in slightly different bending moment stiffness and resistance of the fuses within the same floor level, since the width of the concrete slab for the exterior beams was approximately half of that for the interior beams. The steel grade assigned to the flange and web fuse plates is S235.

Tables 3 and 4 give the details of the dissipative fuses introduced in the interior and exterior frames and their placement in the case study structures, respectively. The fuses were located half a meter from the columns. The rebar and beam gaps were of 60 mm, whereas the free and total lengths of the web and flange plates were of 220 and 600 mm, respectively. Two 270*4 mm² web steel plates and a 270*14 mm² flange steel plate of grade S355 were used to reinforce the composite steel-concrete beam adjacent to the fuses. These plates extended for half a meter in the interior frames and one meter in the exterior frames to prevent damage from spreading into the unreinforced beam zones.

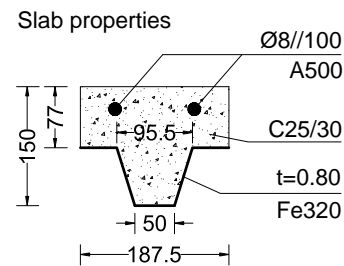


Fig. 9 Properties of the steel-concrete slab (in MPa, mm)

Table 3 Dimensions for the dissipative fuses (mm, mm²)

Frame	Rebars in effective width	Fuse ID	Flange plate	Web plates
Exterior	8Φ20	fe1	200*14	2x 220*4
		fe2	200*12	2x 210*4
		fe3	180*12	2x 210*4
		fe4	170*10	2x 200*4
Interior	10Φ20	fi1	230*14	2x 220*4
		fi2	230*12	2x 210*4
		fi3	200*12	2x 210*4
		fi4	180*10	2x 200*4

Table 4 Placement of the dissipative fuses

Floor where applied	Case study					
	2-W1	2-W2	4-W1	4-W2	8-W1	8-W2
1						
2	fe3, fi3	fe3, fi3		fe1, fi1		fe1, fi1
3		fe4, fi4	fe1, fi1	fe2, fi2		fe1, fi1
4				fe4, fi4		fe1, fi1
5					fe1, fi1	fe1, fi1
6						fe2, fi2
7						fe3, fi3
8						fe4, fi4

Fig. 10 gives the sagging (α^+) and hogging (α^-) bending moment resistance ratio of the dissipative fuses to the structural beam [Eq. (19)]

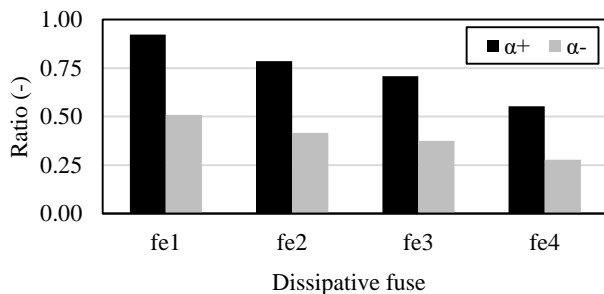
$$\alpha^{+(-)} = \frac{M_{Rd,max,fuse}^{+(-)}}{M_{Rd,beam}^{+(-)}} \quad (19)$$

where $M_{Rd,max,fuse}^{+(-)}$ is the maximum sagging (hogging) bending moment resistance of the dissipate fuse and $M_{Rd,beam}^{+(-)}$ is the sagging (hogging) moment resistance of the composite structural beam.

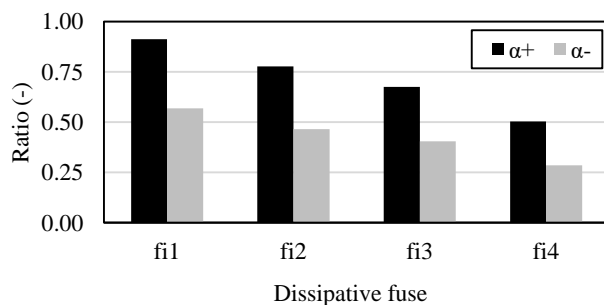
Fig. 10 shows that α^- is consistently lower than α^+ . This is likely due to the reduction in hogging moment resistance of the dissipative fuses, which is caused by the onset of the plate buckling mechanism.

Furthermore, the resistance value used in the calculation of α^+ was the ultimate sagging bending moment resistance of the dissipative fuse, at which point the steel of the flange fuse plate has suffered considerable strain hardening, further highlighting the discrepancy between α^+ and α^- . The values of α^+ and α^- also suggest that the hogging moment should be the governing parameter in the design of moment-resisting frame structures equipped with the dissipative fuses.

Sagging resistance ratios up to 0.92 were considered, which, according to Calado *et al.* (2013), may suggest that damage is not limited to the fuse sections. It should be noted that the ratio compares the bending moment resistance of the dissipative fuse and that of the unreinforced composite beam. However, the beam zones that are in fact adjacent to the dissipative fuses are reinforced with additional steel plates, whose detailing is at the discretion of the designer. As a result, a detailed assessment of the seismic bending moment diagram



(a) External dissipative fuses



(b) Internal dissipative fuses

Fig. 10 α^+ and α^- of the designed dissipative fuses

obtained by the development of maximum resistance in the dissipative fuses at each end of the structural beam was performed, providing information on the design of the reinforcing steel plates as well as how long they should be to prevent damage in the unreinforced beam zones. This ensured that, even with sagging moment resistance ratios of up to 0.92, the non-dissipative beam components should not present damage.

Gravity loads were quantified following the guidelines in EN1990 (Eurocode 2002) for office type buildings. The resulting gravity loads for each service floor and the roof were 3283 kN and 2592 kN, respectively. For the response spectrum and nonlinear static analyses, earthquake action was based on the type 1 response spectrum described in EN1998-1 (Eurocode 2004b) with peak ground accelerations (PGA) of 0.15 g, 0.3 g and 0.5 g.

Type C soil, class II importance factor and viscous damping ratio of 2% were assumed for the soil conditions, structural importance and damping behaviour, respectively. The assumption of 2% for the viscous damping ratio was deemed conservative and appropriate for the presented case studies. This is because the dissipative components were mainly of steel (i.e., steel plates, rebars and columns). Evidently, the concrete slab would likely provide some additional damping, in which case a viscous damping ratio of 5% could be considered instead.

For the nonlinear time history analyses, the aforementioned response spectrum (associated to a PGA of 0.15 g) was used to artificially generate three different accelerograms using the computer code SIMQKE (Gasparini and Vanmarcke 1976). These three accelerograms, whose response spectra are illustrated in Fig. 11, were then scaled such that the structures could be assessed for the chosen PGAs of 0.15 g, 0.3 g and 0.5 g.

The structures were simulated in SAP2000 (CSI) using beam type elements. The joints of the steel frames (i.e. connection between main beams and columns) were modelled as rigid joints, whereas the supports of the secondary beams were modelled as pinned connections. Boundary conditions representing the foundations were assumed to be fully fixed. Each storey was considered to be functioning as a rigid in-plane diaphragm and, as discussed previously, planar numerical assessment was carried out, reducing the number of degrees of freedom per storey to three.

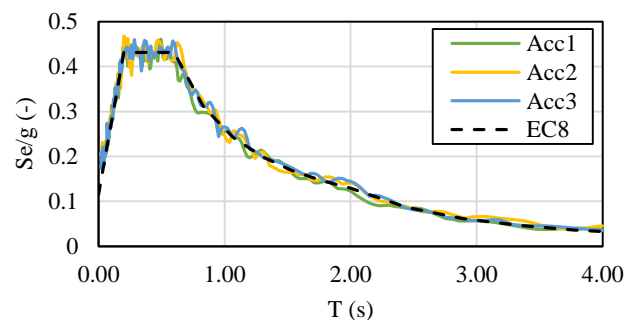


Fig. 11 Response spectrum of the artificially generated accelerograms

Two approaches were used to model the hysteretic behaviour of the dissipative fuses and of the structural beams: plastic hinges and link elements. Despite this, the responses predicted by the two approaches were assessed to guarantee that the preference in choice was merely due to convenience in obtaining the results from SAP2000 (CSI). Indeed, both approaches provided the same results regardless of the type of analysis performed. In the plastic hinge approach, SAP2000 (CSI) allows the visualisation of the sequence of the formation of the plastic hinges, whereas the link element approach, which was used in the nonlinear time history analyses, allows for the automatic calculation of the dissipated energy. The hysteretic behaviour of the dissipative fuses was determined using the analytical model proposed in the present article. The nonlinear properties of the columns and the composite steel-concrete beams were defined following the FEMA 356 recommendations on interacting P-M and moment hinges, respectively (FEMA 2000).

It was also important to define the appropriate hysteresis for the composite steel-concrete beams in order to obtain fairly realistic comparisons of energy dissipation between conventionally designed structures and those equipped with the dissipative fuse. Outcomes from the experimental testing of composite steel-concrete beam-column connections performed by Calado *et al.* (2000) showed that the hysteresis shape for exterior and interior columns is similar to that obtained using pivot and kinematic hysteresis models, respectively. Therefore, these models were assumed for the link elements located near the exterior and interior columns of the frames.

Fig. 12 gives the resulting moment-rotation envelopes of the interior dissipative fuses and the steel-concrete beam. For the analysis of conventional structures, the sagging moment of the steel-concrete beam was conservatively limited to the hogging moment resistance.

With such assumption, it should be noted that a direct comparison between the sagging moment resistances of dissipative fuses and the steel-concrete beam should not be made in Fig. 12. The ratio α^+ was calculated with reference to the sagging moment resistance of the steel-concrete beam considering the contribution of concrete in compression. Furthermore, the abovementioned comparison could also lead to the perception that the fi1 and fi2 dissipative fuses presented higher sagging moment resistances compared to the steel-concrete beam, under which the dissipative fuses should not be able to limit the spread of damage. Recalling the discussion previously presented, additional steel plates were used to reinforce the zones of the steel-concrete beam adjacent to the dissipative fuses such that these zones would always remain elastic, regardless of being under both hogging and sagging moments.

The conventional structures would likely present slightly higher stiffness and increased base shear as consequences, respectively, of the higher initial stiffness and hogging moment resistance (the governing resistance parameter) of the conventional steel-concrete beams.

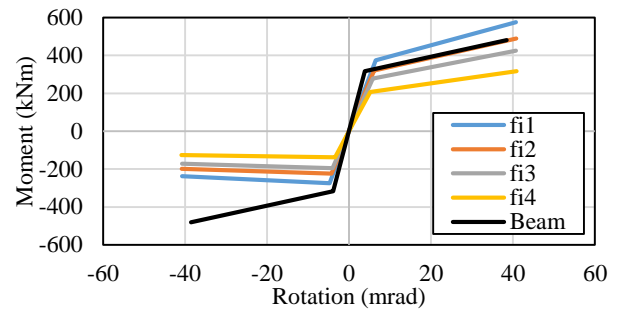


Fig. 12 Moment-rotation envelopes of the interior dissipative fuses and the steel-concrete beam

5. Result assessment

5.1 Response spectrum analyses

According to the procedure described in section 3, a behaviour factor of four was assumed for all case studies. Fig. 13(a) illustrates the fundamental vibration periods for the case studies and suggests that for all three dissipative configurations (C, W1 and W2), the fundamental period approximately doubles when the number of storeys is doubled. Structures with W2 dissipative configuration had the highest periods due to the introduction of weaker dissipative fuses, which in turn reduces the global stiffness of the structures.

Notwithstanding, the differences in values between dissipative configurations were minimum, which may be because dissipative fuses with maximum capacity ratios up to 0.92 were introduced, providing rotational stiffness in the order of that presented by the composite steel-concrete beams. Fitting reinforcing steel plates to prevent the spread of damage was also responsible for the attenuation of period increment due to the installation of the fuses. The similarity in fundamental periods suggests that a re-design of the structures following the introduction of the dissipative fuses is not required.

Similar trends are reported for the maximum drift sensitivity coefficient in Fig. 13(b), since it also depends on the global stiffness of the structures. Maximum drift occurred at the first, second and third floors for 2-, 4- and 8-storey buildings, regardless of the dissipative configuration. All values were below 0.2, at which point EN1998-1 (Eurocode 2004b) disregards the need to perform nonlinear analyses to assess the second order effects occurring within the structures. However, since 8-storey buildings had values of maximum inter-storey drift sensitivity coefficient above 0.1, the internal forces and moments due to the applied seismic action should be amplified by the factor $1/(1 - \theta)$, with θ being the maximum inter-storey drift sensitivity coefficient.

The difference in the sensitivity coefficient between the W1 and W2 dissipative configurations was almost negligible. The change in dissipative fuses from the W1 to W2 configurations mainly occurred at the upper levels of the structures, which should not have a significant influence on the stiffness of the storey where the maximum drift sensitivity values were observed.

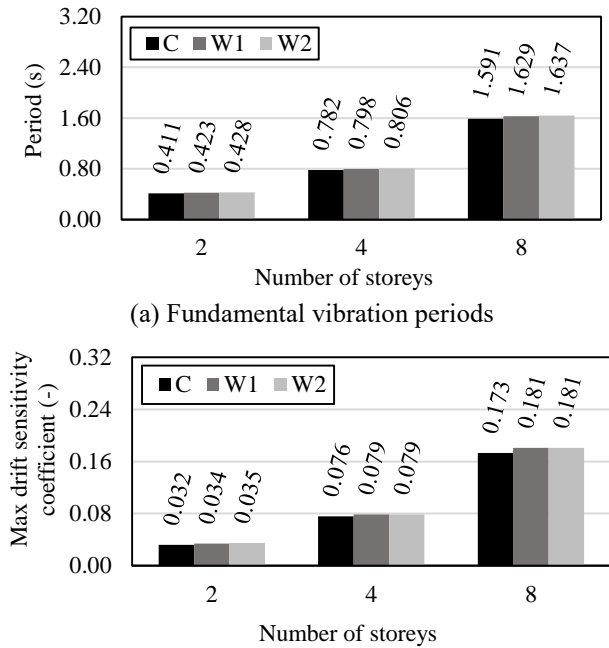


Fig. 13 Outcomes from response spectrum analyses

The continuous rise in the drift sensitivity coefficient with taller buildings, signifying the increase in global flexibility of the structure, eventually leads to moment-resisting frame structures becoming less efficient at resisting earthquakes. In these cases, structural members are designed to satisfy drift related issues rather than to achieve the necessary resistance. Furthermore, the resulting structural members are usually economically inviable.

The use of dissipative fuses to match the demand in resistance might slightly improve the aforementioned problem, but the associated bending moment resistance ratio α is generally very low, which, according to previous research considerably compromises the energy dissipation capability (Castiglioni *et al.* 2012, Calado *et al.* 2013). The application of these dissipative fuses therefore seems to be limited to low- and mid-rise moment-resisting frame structures. However, their potential can still be exploited in high-rise structures if moment-resisting frame structures equipped with dissipative fuses are used in combination with other lateral force resisting systems.

The ratio between the bending moment resistance of the dissipative member/fuse and the acting bending moment defines the overstrength ratio

$$\Omega = \frac{M_{Rd,dissipative\ member(fuse)}}{M_{Ed}} \quad (20)$$

The ratio provides an overview of the amount of reserve resistance the members/fuses have under a certain level of applied seismic action and is relevant for the design of non-dissipative structural members based on capacity design principles. Indirectly, the ratio can also shed light on the design efficiency of the dissipative members/fuses for the imposed design conditions (e.g., structural height, applied seismic force, behaviour factor).

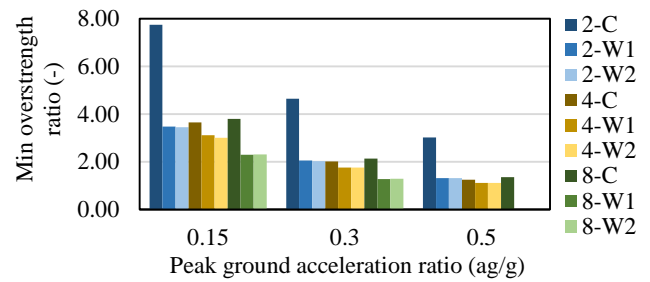


Fig. 14 Minimum overstrength ratios

Fig. 14 provides the minimum overstrength ratios for each structure and PGA, whose values were calculated based on the hogging bending resistance of the dissipative members/fuses. Since the design was mainly aimed for a PGA of 0.5 g, the overstrength ratio increases with smaller PGAs. Especially for a PGA of 0.15 g, the overstrength was such high that most structures remained likely elastic.

It is noteworthy that apart from using a PGA much lower than that intended initially, the assumption of a constant behaviour factor also greatly contributed to the difference between acting and resisting bending moments. To attain lower overstrength ratios, either the structures should be designed for lower lateral force resisting capacities or a smaller behaviour factor may be applied, reducing ductility demand by compensating in strength.

Contrary to the 8-C structure, the 8-W1 and 8-W2 structures had overstrength ratios below unity for an applied PGA of 0.5 g. Such values were omitted in Fig. 14 (and later in Fig. 15), since overstrength ratios below unity suggest that the 8-W1 and 8-W2 structures had failed. The occurrence of failure might be associated to the amplified acting internal forces and moments, which had accounted for the second order effects, and to the large reduction in hogging bending moment resistance due to the introduction of the dissipative fuses.

According to these results, a re-design should be carried out, either by increasing the structural beams and columns cross sections of the structure to cope with any rise in bending moment resistance of the dissipative fuses (lower α) or by compensating for the lack of lateral force resisting capacity with an additional system such as bracing, shear wall or another solution. As noted previously, the first approach is probably limited to a maximum building height, after which the design is so inefficient that the structural members are no longer economically viable.

Notwithstanding, the verification of the 8-W1 and 8-W2 structures for an applied PGA of 0.5 g maybe conservative. Verification was performed by conservatively comparing the design bending moment against the hogging bending resistance of the dissipative fuses, regardless of the sign of the design moment (sagging or hogging).

Consistent reduction in overstrength was observed for the W1 and W2 dissipative configurations, with the greatest declines reported for 2-storey buildings. This was likely associated to the initial use of fe3 and fi3 fuses in the 2-storey buildings as opposed to the 4- and 8-storey structures, which used fe1 and fi1 fuses. Differences in

minimum overstrength ratio between W1 and W2 dissipative configurations were small, since changes in dissipative fuses in the W2 configuration were mainly aimed at reducing the higher overstrength ratios occurring in the top storeys of the structures.

Fig. 15 illustrates the ratio of maximum to minimum overstrength registered within each structure

$$\text{Indicator for global dissipative behaviour} = \frac{\max \Omega}{\min \Omega} \quad (21)$$

The ratio, identical to that given in EN1998-1 (Eurocode 2004b) for bracing, assesses whether the dissipative fuses employed in the various storeys yield and dissipate energy at approximately the same time or in a phased manner, thus providing an overview of the global dissipative behaviour of the structure. Higher ratios represent structures with phased dissipation, whereas lower ratios indicate homogeneous dissipative behaviour.

Provided that structural detailing is identical throughout the storeys, the ratio tends to increase with increasing structural height, associated with the higher gradient of the acting bending moment. Furthermore, the highest ratios were found for the conventional building configurations. The application of a single dissipative fuse for the whole structure (W1 configuration) did not affect the ratio substantially, since the distribution of bending moment resistance remained uniform in the vertical direction. However, for W2 configurations where an effort has been made to adjust the bending moment resistance to the acting values, a remarkable drop in the ratio was achieved, limiting its value under 1.40 for all building heights.

5.2 Nonlinear static pushover analyses

Pushover analyses, considering geometric nonlinearity, were carried out by applying a lateral load distribution proportional to the first mode of vibration. Control point displacement was defined as the roof displacement. Fig. 16 illustrates the pushover curves of the case studies and the corresponding structural performance points for all PGAs. The performance points were determined following the N2 method as described in annex B of EN1998-1 (Fajfar and Fischinger 1988, Eurocode 2004b).

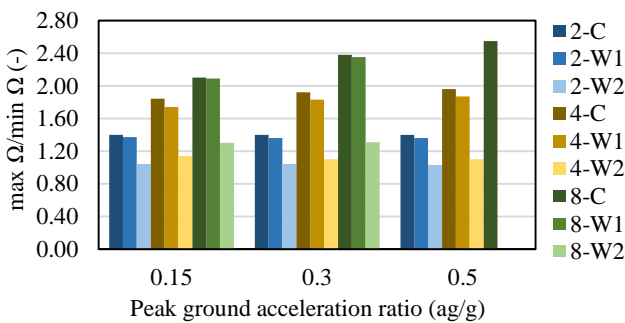
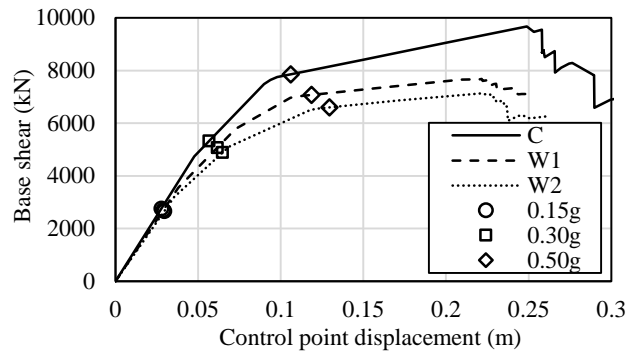
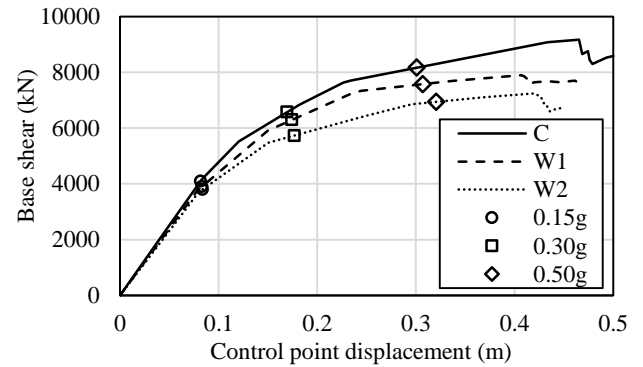


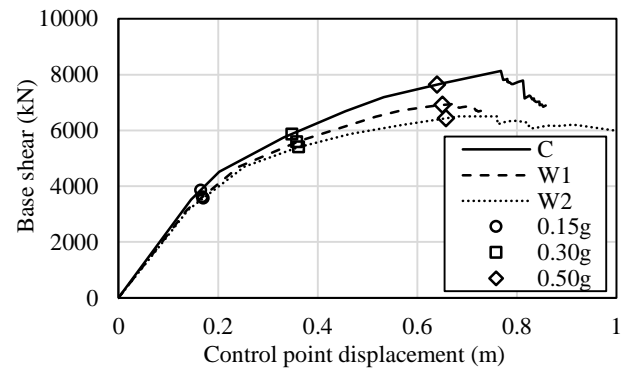
Fig. 15 Indicator for global dissipative behaviour



(a) 2-storey structures



(b) 4-storey structures



(c) 8-storey structures

Fig. 16 Nonlinear static pushover curves of the case studies

Some results confirm the findings presented in the last sub-section: i) the reduction in initial stiffness between dissipative configurations (C, W1 and W2) was minimal but of the same order as reported previously; and ii) all structures remained essentially elastic for a PGA of 0.15g. However, contrary to the outcomes based on response spectrum analyses, the performance point of 8-W1 and 8-W2 structures, calculated for a PGA of 0.5 g, suggests that the structures were able to withstand the earthquake. This could be due to the exploitation of capacity reserve provided by the sagging branch of the dissipative fuses through further redistribution of forces.

A general decreasing trend from C to W2 configuration can be seen for the base shear, which can be attributed to the progressive weakening of the members responsible for energy dissipation (structural beam or dissipative fuses).

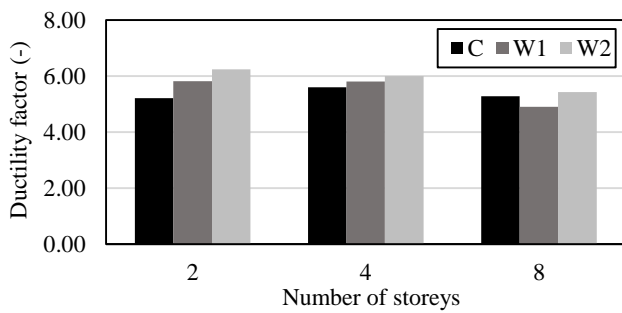


Fig. 17 Ductility factor

However, the displacement capacity represented by the control point displacement at the drop of base shear was reduced for both W1 and W2 structures. This may be due to the lower hogging bending moment resistance of the fuses, which precipitated the onset of structural yield and mobilisation of ductility.

The reduced displacement capacity does not imply that the global ductility of the structure is lower for W1 and W2 building configurations. Fig. 17 illustrates the global ductility factor determined for all structures. The global ductility factor evaluates the plastic displacement capacity that the structure can provide up to the achievement of the plastic mechanism and is defined as the ratio between the roof displacement at the activation of the plastic mechanism and the displacement at first yield. The values show that the global ductility of W1 and W2 dissipative configurations was higher than that of the conventional structure for 2- and 4-storey buildings. For 8-storey buildings, ductility factor decreased when switching from C to W1 configuration.

In the 8-W2 structure, the adjustment of the bending moment resistance to the acting values improved global ductility and displacement capacity of the structure by allowing the top-level dissipative fuses to yield and develop large rotations.

Fig. 18 compares the plastic hinge distribution of the 8-C, 8-W1 and 8-W2 structures at the performance point of 0.5 g PGA (θ_y and θ_u are the yield and ultimate rotations, respectively). All structures exhibited a desirable global plastic hinge distribution, with plastic hinges developing at the beam ends and at the base of the ground level columns.

Inelastic behaviour has been successfully limited within the dissipative fuses in the structures with W1 and W2 dissipative configurations.

The number of plastic hinges and the extent of their development increased from 8-C to 8-W2 structures. Particularly, with respect to the formation of plastic hinges, the effects due to the adjustment of the fuse resistance to the design bending moment were most notable at the top floors.

With the larger extent of plastic hinge development, the 8-W2 structure is expected to present an improved performance in terms of energy dissipation. This observation is subsequently confirmed by the results of the nonlinear time history analyses presented in subsection 5.4.

Plastic hinges which exhibited maximum rotations are mainly located on the second and third floors. A possible reason is that the assumed base column boundary conditions

(fully fixed) usually shifts the maximum rotations to the upper floors. The reduction in bending moment resistance of the fuses in W2 structures would likely contribute to a further upward shifting of the said maximum rotations.

Similar trends can be observed for the 2- and 4-storey structures in terms of global plastic hinge distribution and limitation of inelastic behaviour within the dissipative fuses. All plastic hinges either representing the structural beam or the dissipative fuses reached yield rotation in every 2- and 4-storey structures. Maximum rotations occurred in plastic hinges located on the first and second floor for the 2- and 4-storey structures, respectively.

5.3 Behaviour factor assessment

The applicability of the behaviour factor in current design regulations is only limited to a small range of structures, in which the presented structures are not included.

In this respect, Castiglioni *et al.* (2017) has recently proposed a procedure to quantify the behaviour factor of structures based on their nonlinear static pushover response.

According to the quantification procedure, the behaviour factor can be estimated based on Eq. (22)

$$q = q_{\mu} \cdot q_{\Omega} \cdot q_{\zeta} \quad (22)$$

where q_{μ} , q_{Ω} and q_{ζ} are the displacement, overstrength and damping dependent factor, respectively. The damping dependent factor is equal to 1.0 when assuming the same damping ratio for elastic and nonlinear analysis.

The above factors depend on individual variables of the pushover curve namely, i) the considered maximum displacement, ii) the force chosen as the first yield of the structure and iii) the force and displacement resulting from the assumption of an equivalent elastic-perfectly plastic response. As suggested by Castiglioni *et al.* (2017), different approaches maybe adopted to determine the value of these variables.

The combination of the different approaches resulted in 90 methods for the quantification of behaviour factor, from which Castiglioni *et al.* (2017) identified those optimum for a target behaviour factor of 4.0. The ensuing optimized methods (1, 5, 16 and 19) are employed herein to assess the validity of the behaviour factors assumed in the linear response spectrum analyses. Further details on the methods used to predict the behaviour factors can be found in Castiglioni *et al.* (2017).

Fig. 19 illustrates the values averaged based on the selected methods for the global, displacement and overstrength dependent factors. Except for structure 2-C, the global behaviour factor obtained for the structures was above 4.0, suggesting that the assumed value in the linear response spectrum analyses was acceptable. Since the behaviour factor of structure 2-C was slightly below the assumed value, a re-verification should be conducted with a behaviour factor lower than the estimated value of 3.68.

Comparing the values of the displacement dependent factor, an increasing trend may be observed when the dissipative configuration of the structure varies from C to W2. The increasing trend is mainly due to the higher

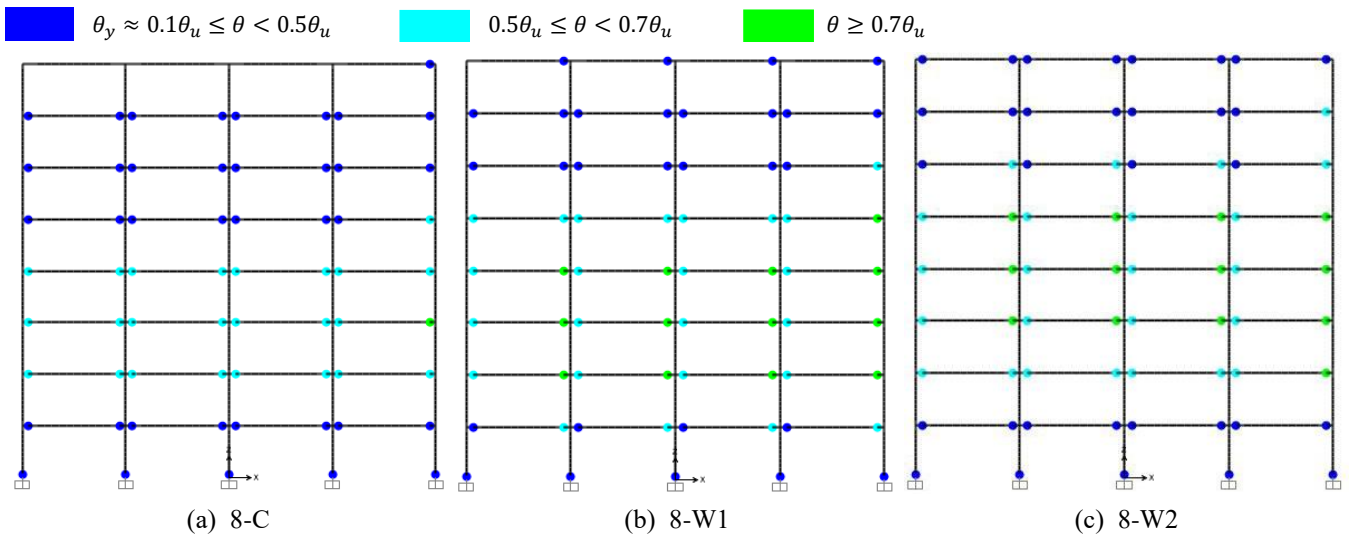
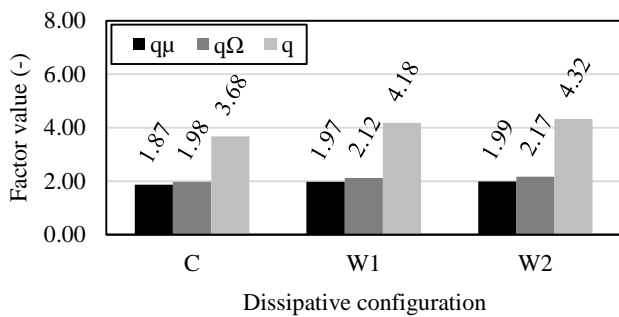
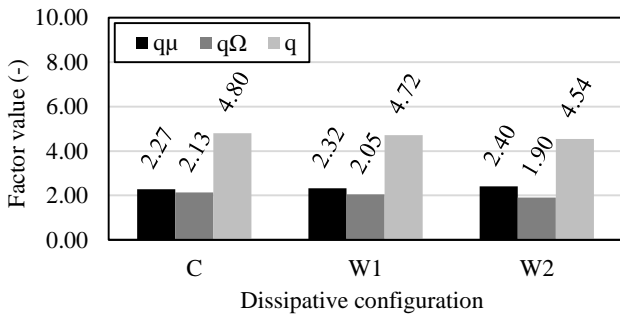


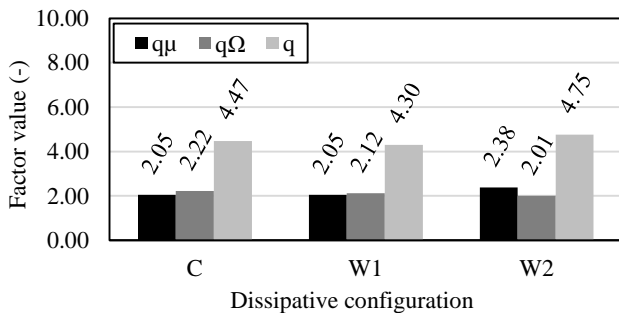
Fig. 18 Plastic hinge distribution of the 8-storey structures at performance point of 0.5g PGA



(a) 2-storey structures



(b) 4-storey structures



(c) 8-storey structures

Fig. 19 Evaluation of behaviour factor

rotational capacity of the dissipative fuses in relation to that provided by the structural beam. Notwithstanding, the displacement dependent factor is also likely to be influenced by the distribution of plastic hinges along the height of the structure. W2 structures developed a larger number of plastic hinges than W1 structures, therefore increasing the ultimate deformation capacity.

A general trend cannot be established for the global behaviour factor, since it depends on the displacement and overstrength dependent factor. As discussed, the displacement dependent factor usually increases from C to W2 dissipative configuration. However, the same cannot be concluded for the overstrength dependent factor, as the replacement of the structural beam by the welded dissipative fuses as the dissipative component generally causes a decrease in the global overstrength of the structure.

5.4 Nonlinear time history analyses

The maximum response obtained from the three accelerograms was considered for the values of maximum roof displacement, base shear force and maximum and residual inter-storey drift, whereas averaged values were considered for the dissipated energy.

5.4.1 Maximum roof displacement and base shear

Time history outcomes generally presented maximum roof displacement trends similar to those observed from pushover analyses [Fig. 20(a)].

The maximum roof displacement generally increased with higher building heights and for different dissipative configurations in the following order: C, W1 and W2. However, some exceptions were observed for the lowest level of PGA, in which the 2- and 4-storey structures with dissipative fuses presented lower roof displacements than the conventional structure. At that level of PGA, the response of the structures was governed by the global stiffness of the structures rather than by their capacity.

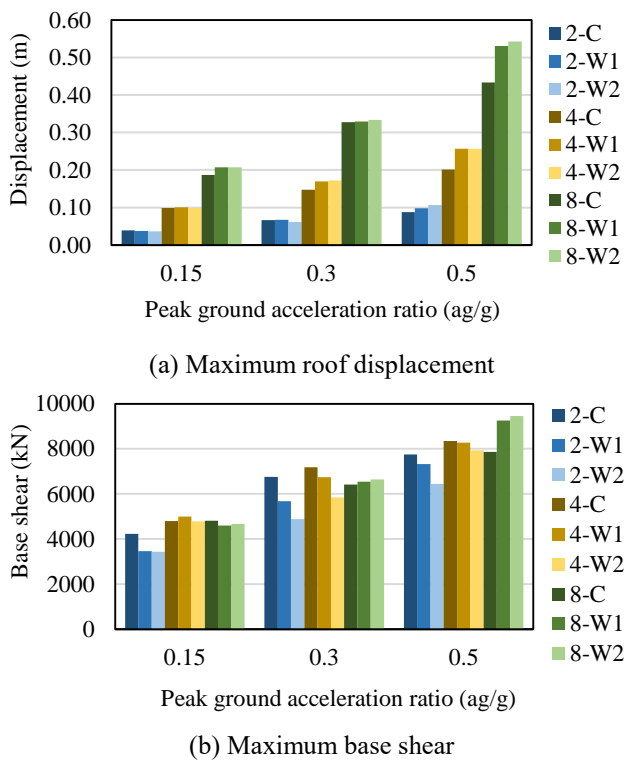


Fig. 20 Outcomes from time history analyses I

Since global stiffness was shown to be very similar between C, W1 and W2 structures in the previous analyses (i.e., linear response spectrum and nonlinear static pushover), a general trend could not be established.

Contrary to what was expected from the pushover outcomes, in which maximum base shear decreases from C to W2 dissipative configuration, a general trend could not be established herein [Fig. 20(b)]. The described trend was mainly valid for 2- and 4-storey structures subjected to PGAs of 0.3 g and 0.5 g. Indeed, the base shears presented herein were not the maximum values that the structures could supply, but rather the responses obtained based on the imposed accelerograms. With respect to the 8-storey buildings, another possible cause of the said discrepancy could be the influence of higher order modes of vibration. For lower structural heights, structural behaviour is essentially governed by the fundamental mode of vibration. As such, the response between pushover and time history analyses would not differ much. For higher structural heights, the participation of higher order modes of vibration, which were not captured in the pushover analyses, would result in larger differences between the pushover and time history outcomes.

5.4.2 Development of plastic hinges

Further evidence on the influence of higher order modes of vibration can be illustrated based on the plastic hinge distribution obtained from time history analyses.

Fig. 21 illustrates the plastic hinge distribution of the 8-storey structures at maximum base shear (PGA=0.5 g). Comparing Figs. 18 and 21, the maximum rotations

observed at the lower floors of the structure were smaller for time history analyses. Furthermore, the location of maximum rotations seemed to be slightly shifted upwards, this being most remarkable for the 8-W2 structure. Distribution of forces along the height of the structure usually varies with the consideration of the contribution of higher order modes of vibration, leading to the increase of internal forces in the upper floors. In particular, such increase in combination with the reduced moment resistance of the dissipative fuses in the 8-W2 structure led to the observation of maximum plastic hinge rotations at the 7th floor of the 8-W2 structure.

The increase in the base shear force for the 8-W1 and 8-W2 structures when compared with the conventional counterpart (8-C) seems to contradict the perception that the structures with dissipative fuses are more deformable and therefore should present lower spectral accelerations. Notwithstanding, the more generalized spread of plastic hinges and the corresponding higher rotation levels developed in 8-W1 and 8-W2 structures, as shown in Fig. 21, led to a significant increase in lateral displacements (shown in Fig. 20(a)) compared to the 8-C structure. As a result, this significant increase in lateral displacements also led to increased base shear forces. This apparent contradiction was not observed in the 2- and 4-storey structures, where the three types of structures (C, W1 and W2) developed a more comparable spread of plastic hinges and corresponding rotation levels.

5.4.3 Maximum and residual inter-storey drift

Maximum and residual inter-storey drift (Fig. 22) are given by the difference in displacement between consecutive floors divided by the corresponding floor height. Similar to the conclusions made based on the maximum roof displacement, the values obtained for maximum inter-storey drift also seemed to indicate that drift values increase with less rigid and resistant structures. This was evidenced by the drift values registered for the structures with more storeys and with W1 and W2 dissipative configurations. Furthermore, the difference in maximum drifts between structures with different dissipative configurations (C, W1 and W2) was more remarkable when the structures were subjected to higher PGAs.

Maximum inter-storey drift values were registered at the 2nd storey (between first and second floors) for the 2- and 4-storey structures. However, the 4-W2 structure exhibited maximum inter-storey drift at the 3rd storey (between second and third floors), which may be caused by the stiffness reduction at the top floors from the use of dissipative fuses with lower resistance capacity. For 8-storey structures, with the exception of the 8-W2 structure, the storey at which maximum inter-storey drift was observed shifted from the 3rd storey to the 5th storey (between fourth and fifth floors) with increasing PGAs. The 8-W2 structure exhibited maximum inter-storey drifts at the 7th storey (between sixth and seventh floors) likely due to the same conclusions made for the 4-W2 structure.

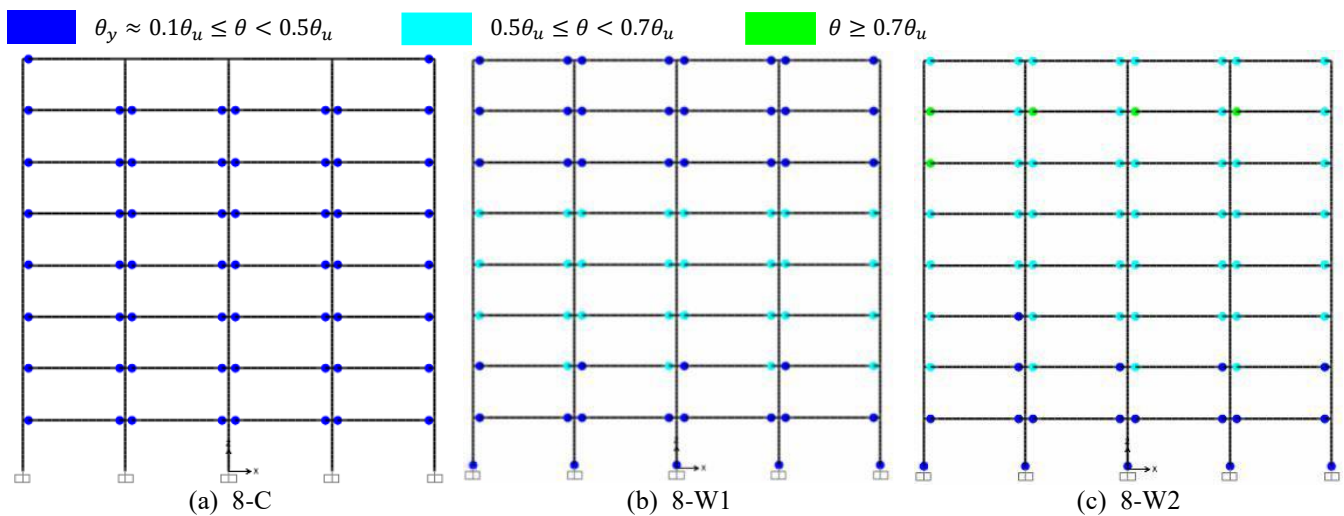


Fig. 21 Plastic hinge distribution at maximum base shear of the 8-storey structures under 0.5g PGA

The inter-storey drift can also implicitly serve as an indicator to whether the plastic hinges have exceeded their ductility limits. In this case, all maximum inter-storey drifts were below 3%, which implicitly correspond to plastic hinge rotations below 30 mrad. Therefore, none of the plastic hinges exceeded the corresponding ductility limits, suggesting that no structure had collapsed.

Residual inter-storey drifts provide a general idea on the reparability of the structure after an earthquake. All structures presented a residual drift below a recommended limit of 0.5%. The limit of 0.5% is considered by McCormick *et al.* (2008) as the acceptance criteria for performance-based seismic design. A residual drift exceeding this threshold was shown to cause discomfort to the occupants of the structure and usually not to be financially viable for reparation.

Comparing values under different levels of PGAs, the registered residual inter-storey drift was lowest under a PGA of 0.15 g, in which the structures remained essentially elastic. The residual inter-storey drift also seemed to be lower in the structures equipped with dissipative fuses, which agreed with the outcomes presented in Valente *et al.* (2017a). Two possible reasons to this observation could be: i) the inherent characteristics of pivot hysteresis, which compared to the kinematic hysteresis, led to smaller residual rotations subsequent to unloading; and ii) plastic hinges of the ground floor columns generally developed slightly higher inelastic deformations in the conventional structures compared to the structures equipped with dissipative fuses. These observations suggest that structures equipped with dissipative fuses provide enhanced re-centring capabilities compared to the conventional structures. Indeed, the structural beams of the conventional structures suffered permanent and irreparable damage following an earthquake. In the structures equipped with dissipative fuses, though the plates of the fuses may be damaged, the slightly enhanced re-centring capacity of these structures could potentially ease the replacement process of the fuse plates.

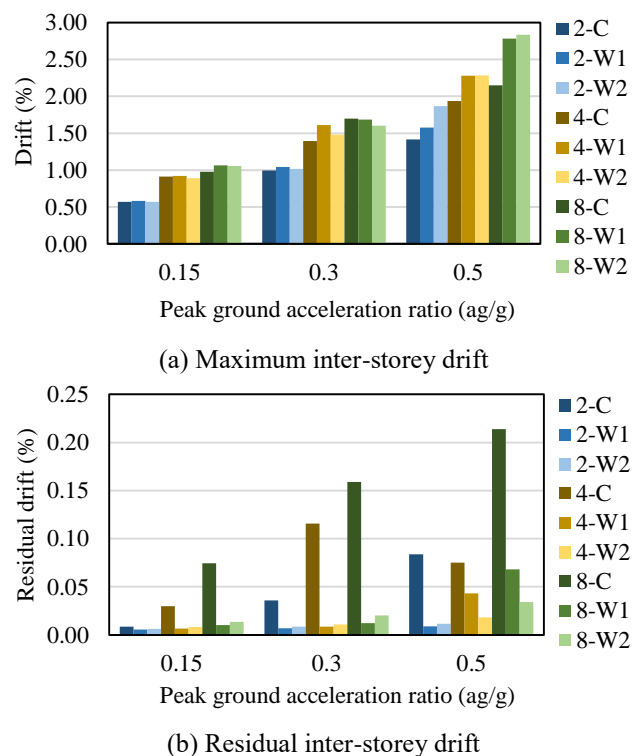


Fig. 22 Outcomes from time history analyses II

5.4.4 Average energy dissipated

Regarding the average energy dissipated by the dissipative elements (Fig. 23), it should be noted that the plastic hinges assigned to the columns either suffered negligible plastic deformations or remained elastic for all structures and under all PGAs.

Furthermore, inelastic deformation was limited to the dissipative fuses in W1 and W2 structures, without any development of plastic hinges at the remaining areas of the structural beam. In this respect, the values presented in Fig.

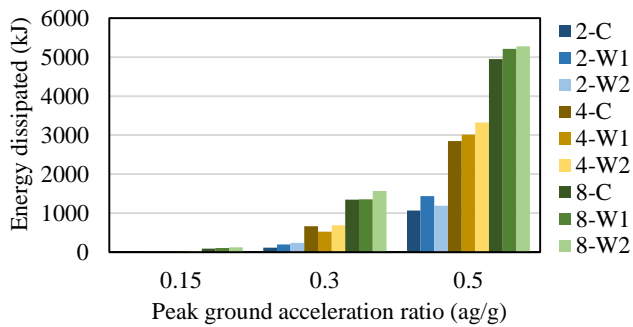


Fig. 23 Average energy dissipated

23 only represent the dissipated energy either from the structural beam (C type structures) or from the dissipative fuses (W1 and W2 type structures).

The total energy dissipated by the structures depends on the number of plastic hinges mobilised, the extent of inelastic deformations and the type of hysteresis. Since most of the dissipative components remained essentially elastic under a PGA of 0.15 g, the total dissipated energy by these components was approximately zero for most structures. A small amount of energy was dissipated for the 8-storey structures, which can be attributed to the initiation of yielding.

The amount of energy dissipated generally increased with structural height and with the dissipative configurations in the following order: C, W1 and W2. Indeed, the increased number of storeys provided additional structural components to dissipate energy. Furthermore, the decrease in bending moment resistance due to the introduction of the welded dissipative fuses also precipitated the formation of plastic hinges, potentially improving the energy dissipation performance of the structure. As such, despite the dissipative fuses presenting a hysteretic behaviour with pinching phenomenon, the global dissipation performance of the structures with dissipative fuses was higher than that exhibited by the conventional structure, in which its dissipative component presents a bilinear hysteretic behaviour.

6. Conclusions

This research provided a design-oriented assessment of composite steel-concrete frame structures equipped with welded dissipative fuses. A revision and calibration of the existing analytical models to characterise the hysteretic behaviour of the dissipative fuse was first undertaken. The relationship was then implemented within lumped plasticity models to assess the seismic behaviour of moment-resisting frame structures equipped with the dissipative fuses being possible to draw the following conclusions:

- Fairly good agreement was achieved between the predictions from the analytical model and the experimental hysteretic curves. However, neglecting the web fuse plates in the calculation of bending moment resistance implies that model accuracy is

dependent on the strength the web plates are able to contribute to the bending moment. In this respect, it is recommended that the web plates should be designed in accordance with the size of the flange fuse plate or a higher overstrength factor should be applied to the design forces of the non-dissipative elements.

- Results from linear response spectrum, pushover and time history analyses reveal that the dissipative fuses successfully prevented the spread of damage to the adjacent structural beam. Assessment of the plastic hinge distribution for all case studies reveals that the structures presented a desirable global plastic hinge distribution. Furthermore, the fundamental period, the maximum roof displacement and inter-storey drifts generally increased with building height and with the dissipative configurations in the following order: C, W1 and W2, whereas a decreasing trend was observed for the base shear. The use of dissipative fuses, whose rotational stiffness and resistance were slightly lower than those provided by the structural beam, mainly contributed to the aforementioned trends. However, few exceptions were observed in time history analyses.
- Contrary to the results from the response spectrum analyses, pushover and time history analyses showed that the 8-storey structures with W1 and W2 dissipative configurations were able to sustain the loads induced by an earthquake with a PGA of 0.5g.
- The ratio of maximum to minimum overstrength was found to be lowest for the W2 dissipative configuration, suggesting that structures with W2 dissipative configuration should provide the best performance in terms of energy dissipation. The time history analyses confirmed such observations.
- On the basis of the approach proposed in Castiglioni *et al.* (2017), a behaviour factor of four was shown to be appropriate for the range of structures assessed in this research.
- Residual inter-storey drift outcomes suggest that structures equipped with dissipative fuses provide enhanced re-centring capabilities compared to the conventional structures.
- Further to the successful prevention of damage spread to the adjacent structural beams and the apparent enhanced re-centring capability, the possibility of a practical replacement of the welded dissipative fuses suggests that moment-resisting frames equipped with these dissipative fuses provide a promising solution for the design of earthquake-resistant structures. Despite this, a welded solution may appear to be difficult to repair without damaging the structural beam. However, it should be noted that the reinforcement plates added to strengthen the structural beam adjacent to the dissipative fuses also served to mitigate this issue. Successive testing and replacement of web and flange fuse plates performed during the experimental campaign at IST of the University of Lisbon (Calado *et al.* 2013) showed that the strength degradation due to successive replacement of the dissipative fuses was limited to acceptable levels.

Acknowledgments

This article was conducted under the INNOSEIS research project (Innovative Anti-Seismic Dissipative Devices, proposal number 709434), financed by the Research Fund for Coal and Steel of the European Commission.

References

- Balut, N. and Gioncu, V. (2003), "Suggestion for an improved 'dog-bone' solution", *Proceedings of the Conference on Behaviour of Steel Structures in Seismic Areas*, Naples, Italy, June.
- Calado, L., Proença, J.M., Espinha, M. and Castiglioni, C.A. (2013), "Hysteretic behavior of dissipative welded fuses for earthquake resistant composite steel and concrete frames", *Steel Compos. Struct.*, **14**(6), 547-569. <http://dx.doi.org/10.12989/scs.2013.14.5.547>.
- Calado, L., Proença, J.M. and Sio, J. (2017), *Chapter 6, Deliverable 3.2: Volume with pre-normative design guidelines for innovative devices*, INNOSEIS project (RFCS-AM-2015-709434). <http://innoseis.ntua.gr/>.
- Calado, L., Simoes da Silva, L. and Simoes, R. (2000), "Cyclic behavior of steel and composite beam-to-column joints", *Connections in Steel Structures IV*, Elsevier Science.
- Castiglioni, C.A., Alavi, A., Brambilla, G. and Kanyilmaz, A. (2017), "A procedure for the assessment of the behaviour factor for steel MRF systems based on pushover analysis", *Proceedings of the 6th ECCOMAS Thematic Conference on Computational Methods in Structural Dynamics and Earthquake Engineering (COMPdyn 2017)*, Rhodes Island, Greece.
- Castiglioni, C.A., Kanyilmaz, A. and Calado, L. (2012), "Experimental analysis of seismic resistant composite steel frames with dissipative devices", *J. Constr. Steel Res.*, **76** 1-12. <https://doi.org/10.1016/j.jcsr.2012.03.027>.
- CSI SAP2000 *Integrated software for structural analysis & design*, Computer and Structures, Inc., Berkeley, California.
- Dowell, R.K., Seible, F. and Wilson, E.L. (1998), "Pivot hysteresis model for reinforced concrete members", *ACI Struct. J.*, **95** 607-617.
- Engelhardt, M.D. and Sabol, T.A. (1997), "Seismic-resistant steel moment connections: developments since the 1994 Northridge earthquake", *Progress Struct. Eng. Mater.*, **1**(1), 68-77. <https://doi.org/10.1002/pse.2260010112>.
- Engelhardt, M.D. and Sabol, T.A. (1998), "Reinforcing of steel moment connections with cover plates: benefits and limitations", *Eng. Struct.*, **20**(4-6), 510-520. [https://doi.org/10.1016/S0141-0296\(97\)00038-2](https://doi.org/10.1016/S0141-0296(97)00038-2).
- Eurocode (2002), *EN1990:2002 Eurocode 0: Basis of structural design*, European Committee for Standardisation, Brussels.
- Eurocode (2004a), *EN1994-1-1:2004 Eurocode 4: Design of composite steel and concrete structures – part 1-1*, European Committee for Standardisation, Brussels.
- Eurocode (2004b), *EN1998-1:2004 Eurocode 8: Design of structures for earthquake resistance - Part 1: General rules, seismic actions and rules for buildings*, European Committee for Standardisation, Brussels.
- Eurocode (2005), *EN1993-1-8:2005 Eurocode 3: Design of steel structures - Part 1-8: Design of joints*, European Committee for Standardisation, Brussels.
- Fajfar, P. and Fischinger, M. (1988), "N2-A method for non-linear seismic analysis of regular buildings", *Proceedings of the 9th world conference in earthquake engineering*.
- FEMA (2000), *Commentary for the seismic rehabilitation of buildings (FEMA356)*, Federal Emergency Management Agency, Washington, DC.
- Gasparini, D. and Vanmarcke, E.H. (1976), *SIMQKE: A program for artificial motion generation*, Department of Civil Engineering, Massachusetts Institute of Technology, Cambridge, MA.
- Gomes, A. and Appleton, J. (1997), "Nonlinear cyclic stress-strain relationship of reinforcing bars including buckling", *Eng. Struct.*, **19**(10), 822-826. [https://doi.org/10.1016/S0141-0296\(97\)00166-1](https://doi.org/10.1016/S0141-0296(97)00166-1).
- He, X., Chen, Y., Eatherton, M.R. and Shao, T. (2018), "Experimental evaluation of replaceable energy dissipation connection for moment-resisting composite steel frames", *J. Struct. Eng.*, **144**(6), 04018042. [https://doi.org/10.1061/\(ASCE\)ST.1943-541X.0002028](https://doi.org/10.1061/(ASCE)ST.1943-541X.0002028).
- Jiang, Z.Q., Yang, X.F., Dou, C., Li, S.H. and Zhang, A.I. (2019), "Seismic performance of prefabricated corrugated web beam-column joint with replaceable cover plates", *Adv. Struct. Eng.*, **22**(5), 1161-1174. <https://doi.org/10.1177/1369433218807688>.
- Koetaka, Y., Chusilp, P., Zhang, Z., Ando, M., Suita, K., Inoue, K. and Uno, N. (2005), "Mechanical property of beam-to-column moment connection with hysteretic dampers for column weak axis", *Eng. Struct.*, **27**(1), 109-117. <https://doi.org/10.1016/j.engstruct.2004.09.002>.
- Lopez-Barraza, A., Ruiz, S.E., Reyes-Salazar, A. and Bojorquez, E. (2016), "Demands and distribution of hysteretic energy in moment resistant self-centering steel frames", *Steel Compos. Struct.*, **20**(5), 1155-1171. <http://dx.doi.org/10.12989/scs.2016.20.5.1155>.
- Ma, H., Wang, J., Lui, E.M., Wan, Z. and Wang, K. (2019), "Experimental study of the behavior of beam-column connections with expanded beam flanges", *Steel Compos. Struct.*, **31**(3), 319-327. <https://doi.org/10.12989/scs.2019.31.3.319>.
- Mazzolani, F. (2000), *Moment Resistant Connections of Steel Frames in Seismic Areas: Design and Reliability*, CRC Press.
- McCormick, J., Aburano, H., Ikenaga, M. and Nakashima, M. (2008), "Permissible residual deformation levels for building structures considering both safety and human elements", *Proceedings of the 14th world conference on earthquake engineering*, Beijing, China.
- Nakashima, M., Inoue, K. and Tada, M. (1998), "Classification of damage to steel buildings observed in the 1995 Hyogoken-Nanbu earthquake", *Eng. Struct.*, **20**(4-6), 271-281. [https://doi.org/10.1016/S0141-0296\(97\)00019-9](https://doi.org/10.1016/S0141-0296(97)00019-9).
- Oh, S.H., Kim, Y.J. and Ryu, H.S. (2009), "Seismic performance of steel structures with slit dampers", *Eng. Struct.*, **31**(9), 1997-2008. <https://doi.org/10.1016/j.engstruct.2009.03.003>.
- Ozkaynak, H., Khajehdehi, A., Gullu, A., Azizisales, F., Yuksel, E. and Karadogan, F. (2018), "Uni-axial behavior of energy dissipative steel cushions", *Steel Compos. Struct.*, **27**(6), 661-674. <https://doi.org/10.12989/scs.2018.27.6.661>.
- Pachoumis, D.T., Galoussis, E.G., Kalfas, C.N. and Efthimiou, I.Z. (2010), "Cyclic performance of steel moment-resisting connections with reduced beam sections—experimental analysis and finite element model simulation", *Eng. Struct.*, **32**(9), 2683-2692. <https://doi.org/10.1016/j.engstruct.2010.04.038>.
- Plumier, A. (1990), "New idea for safe structures in seismic zones", *LABSE Symposium-Mixed Structures Including New Materials*.
- Plumier, A. (2000), "General report on local ductility", *J. Constr. Steel Res.*, **55**(1-3), 91-107. [https://doi.org/10.1016/S0143-974X\(99\)00079-6](https://doi.org/10.1016/S0143-974X(99)00079-6).
- Sabbagh, A.B., Chan, T.M. and Mottram, J.T. (2013), "Detailing of I-beam-to-CHS column joints with external diaphragm plates for seismic actions", *J. Constr. Steel Res.*, **88** 21-33. <https://doi.org/10.1016/j.jcsr.2013.05.006>.

- Valente, M., Castiglioni, C.A. and Kanyilmaz, A. (2016), "Dissipative devices for earthquake resistant composite steel structures: bolted versus welded solution", *Bull. Earthq. Eng.*, **14**(12), 3613-3639. <https://doi.org/10.1007/s10518-016-0002-9>.
- Valente, M., Castiglioni, C.A. and Kanyilmaz, A. (2017a), "Numerical investigations of repairable dissipative bolted fuses for earthquake resistant composite steel frames", *Eng. Struct.*, **131**, 275-292. <https://doi.org/10.1016/j.engstruct.2016.11.004>.
- Valente, M., Castiglioni, C.A. and Kanyilmaz, A. (2017b), "Welded fuses for dissipative beam-to-column connections of composite steel frames: Numerical analyses", *J. Constr. Steel Res.*, **128**, 498-511. <https://doi.org/10.1016/j.jcsr.2016.09.003>.
- Vasdravellis, G., Valente, M. and Castiglioni, C.A. (2009), "Dynamic response of composite frames with different shear connection degree", *J. Constr. Steel Res.*, **65**(10-11), 2050-2061.
- Yu, Q.S.K. and Uang, C.M. (2001), "Effects of near-fault loading and lateral bracing on the behavior of RBS moment connections", *Steel Compos. Struct.*, **1**(1), 145-158. <https://doi.org/10.12989/scs.2001.1.1.145>.